Distribution of xenon gas exchange rates in dogs

P. K. WEATHERSBY, K. G. MENDENHALL, E. E. P. BARNARD,
L. D. HOMER, S. SURVANSHI, AND F. VIERAS
Naval Medical Research Institute and Armed Forces Radiobiology Research Institute, Bethesda, Maryland 20014

WEATHERSBY, P. K., K. G. MENDENHALL, E. E. P. BARNARD, L. D. HOMER, S. SURVANSHI, AND F. VIERAS. *Distribution of xenon gas exchange rates in dogs.* J. Appl. Physiol.: Respirat. Environ. Exercise Physiol. 50(6): 1325–1336, 1981.—The kinetics of xenon gas uptake and elimination in seven anesthetized dogs were studied by simultaneous external recording of gas concentrations in several thousand anatomic sites during 7-h experiments. The data were analyzed by a previously described method of extracting moments of the distribution of gas residence times. Mean residence times (first moment) varied by more than a factor of 50 within a single animal: the fastest exchange was in the lungs (under 2 min), and progressively slower exchange occurred in the brain, spinal cord, ears, peripheral joints, and shoulder (over 2 h). Variance of the residence time (second moment) was found to approximate four times the mean residence time squared. This ratio was nearly the same throughout the body. Indications of unexpectedly high xenon solubility in the ear and joint regions were also found.

inert gas; gas kinetics; moments of distributions; decompression sickness

NUMEROUS EXPERIMENTAL STUDIES of inert gas exchange have been published in this century. These studies have generally either examined the behavior of one or two anatomic sites or have measured exchange rates in mixed venous or arterial blood, or in expired respiratory gas. These latter methods address the overall response of the body in which the behavior of individual organs has been lost in a complicated physiological averaging process. In addition, nearly all of these studies have employed methods of data analysis that are unsuitable for multiple comparisons of large numbers of gas exchange measurements.

Recently, we have developed a mathematical description of inert gas exchange that uses moments as statistical descriptors of inert gas exchange (20). Our descriptive analysis is well suited to comparisons of large amounts of gas exchange data such as those contained in the present report. The studies reported here include up to 3,000 individual anatomic sites monitored simultaneously in a single dog.

MATERIALS AND METHODS

Experimental techniques. Six mature beagles of both sexes weighing between 10 and 16 kg were used in single experiments; a seventh dog was used in three successive single experiments. The dogs were anesthetized with 25 mg/kg pentobarbital (Nembutal); 50-mg maintenance doses were administered as needed to suppress the corneal reflex. In some instances an X-ray image was taken after the initial anesthesia and positioning of the dog for the study. Endotracheal tubes were inserted, but the dogs were allowed to breathe spontaneously at all times.

A standard clinical gamma camera (Searle Phogamma) with a high-sensitivity, parallel-hole, lead collimator was used to acquire the data. This instrument has a NaI crystal and a 19-photomultiplier array with a 24-cm-diam field of view that allowed spatial resolution of about 0.8 cm in a plane of the camera parallel to the face of the camera.

The resolution depends on the physical characteristics of the collimator and on Compton scatter of photons in tissue through relatively large angles with little energy loss. For example, the 81-keV gamma photon can be scattered at a 45° angle and still be detected by the ±20% pulse-height-analyzer window used in these studies.

The effective depth of field of the detector is determined by several physical factors. The first is the exponential attenuation of the gamma-ray flux when traversing tissue. The loss is 18%/cm in water and a slightly higher value in more dense, higher atomic number substances such as bone. In addition, the flux intensity of any source falls off proportional to the square of the distance between source and detector. These factors interact with the actual depth-distribution of radioisotope at any time. The result is an effective response that is strongest at the animal's skin and decreases with depth into tissue. We estimate that about 90% of the total signal arises within 4 cm of the skin.

During the experiment, gamma pulses were counted and assigned locations in a 64 × 64 spatial matrix. Each point in the experimental record represents response in a wedge of tissue with 15-mm^2 base and several centimeters depth. We corrected point-to-point camera response using a data array obtained from a uniform ^{99m}Tc ("flood") source immediately before the study. Background radiation produced an average of 0.15 counts per minute (cpm) per spatial point. Background was treated as zero in the data analysis.

A shielded rebreathing circuit comprised of a 5-liter gas bag, a CO_2-adsorbent cartridge, and one-way valves was prepared with 25–60 mCi of ^{133}Xe and 4–5 liters of oxygen. The restrained dogs rebreathed from this circuit for a period of 10, 40, or 50 min and then breathed room air for a subsequent 6 h. ^{133}Xe emissions were counted for variable intervals: 10 s after the start and the finish of rebreathing, 1 min for the remainder of the xenon

inspiration, and 3 min for the remainder of xenon washout. About 200 total time intervals were used so that an entire single experiment consisted of 64 × 64 × 200 = 800,000 measurements of count rate. The contents of the rebreathing bag and the dog's expired gases for 30 min after the end of rebreathing were adsorbed on charcoal to prevent background increase and to avoid personnel exposure. During the rebreathing period, total volume in the circuit decreased substantially, but the inspired ^{133}Xe concentration remained constant within 10–20%.

We identified specific anatomic sites in several ways: *a*) eyes, ears, and shoulder and wrist joints were manually located, and the position was recorded in the same manner as the kinetic data using ^{57}Co point sources of radiation; *b*) the endotracheal tube and lungs were located by examining the locations of high radioactivity recorded in the first 30 s of the experiment; and *c*) the major blood vessels, heart, kidney, and bladder were marked by recording sequential 10-s images after intravenous administration of ^{99m}Tc sulfur colloid after the xenon study. The combination of these markers and the X-ray images allowed identification of particular anatomic regions within 1–2 cm under favorable conditions. However, movement of the dog relative to the camera by as little as 2 cm during an experiment produced obvious steps in the gas uptake-elimination curve of single locations. This problem both degraded the spatial resolution and caused major numerical problems when attempts were made to analyze the data of a single such area.

Of the nine experiments, only three produced data of sufficient reliability for a full analysis of all points. The remaining experiments provided kinetic data for a smaller number of anatomic regions that were larger than the movement of the dog.

Data analysis. Most studies of inert gas uptake and elimination have involved data interpretation of curves according to blood flow hypotheses. The numerous theoretical and practical objections to this practice prompted us to develop a statistical description of the data, which have been presented in detail elsewhere (20). Analysis of the data is summarized below.

The behavior of any physiological unit is considered as a variable time retention of gas molecules. This holdup phenomenon can be plotted as a curve of the frequency of a gas molecule that has entered the organ at *time 0*, leaving the organ at a particular time, t, later. This plot is called the residence time function, $f(t)$, and is a probability density function that can be treated like other better known probability density functions, such as the normal or Poisson distributions. In statistics, distributions are commonly described by their moments, which are defined as special integrals

$$M_j = \int_0^\infty t^j f(t)dt \qquad (1)$$

$$m_j = \int_0^\infty (t - M_1)^j f(t)dt \qquad (2)$$

The zeroth moment ($j = 0$), M_0, is simply the area under the curve $f(t)$ and is thus exactly 1. The first moment about the origin, M_1, is the mean of the distribution of residence times and is thus taken as the single time most characteristic of the gas exchange process in the organ. The second central moment, m_2, is called the variance. The square root of the variance, the standard deviation, is a common measure of the "width" of the curve. Higher moments have less intuitive meaning but can be taken as summarizing other aspects of a curve, such as its asymmetry.

To relate the residence time function, $f(t)$, to a set of experimental data, we will consider the specific methods of gas administration and detection in a systematic way. In the present study the original gas concentration at the mouth is a square wave of duration, Δ. Thus, we take the arterial concentration to be a square wave of same duration and concentration, G.

$$X(t) = G(u(t) - u(t - \Delta)) \qquad (3)$$

where $u(t)$ is the unit step function and X is the arterial concentration. At the lungs the gas dissolves in the blood and is carried to the area under study. The actual rate of gas entering the region depends on the inspired concentration, the gas solubility and the arterial flow rate, F, so $Y(t) = FX(t)$. The measurement technique responds to the present amount of gas in the organ $Q(t)$, or equivalently to the total accumulated difference between the rate of gas entering the region, $Y(t)$, and the gas leaving the organ, $Z(t)$, since the start of the experiment

$$Q(t) = \int_0^t (Y(x) - Z(x))dx \qquad (4)$$

The rate of gas leaving the region depends on the convolution of the gas input with the organ residence time function, $f(t)$. Thus the dependence of the experimental data on the experimental and physiological functions is

$$Q(t) = \int_0^t (Y(x) - Y(x)*f(x))dx \qquad (5)$$

where * is the symbol for the convolution operation. One must then choose an appropriate form for the residence time probability density function. The function is restricted to have a unit area, that is, all values of probability sum to 1.

$$\int_0^\infty f(t)dt = 1.0 \qquad (6)$$

The most common function used in gas exchange work is a series of exponential terms

$$f(t) = \sum_{i=1}^{n} B_i \exp(-t/\beta_i) \qquad (7)$$

with $\sum_{i=1}^{n} B_i\beta_i = 1$ to satisfy *Eq. 6*. This produces the following expression for the present set of experiments

$$Q(t) = GF(u(t)\phi(t) - u(t - \Delta)\phi(t - \Delta)) \qquad (8)$$

where

$$\phi(t) = \sum_{i=1}^{n} B_i\beta_i^2[1 - \exp(-t/\beta_i)]$$

A more detailed derivation has been published previously

(20). *Equation 8* gives the expected shape of the tissue xenon content curve as a function of the residence time distribution parameters. These parameters of f(t) can then be substituted into *Eqs. 1* and *2* for obtaining estimates of the moments.

$$M_1 = \sum_{i=1}^{n} B_i\beta_i^2 \qquad (9)$$

and

$$m_2 = 2\left(\sum_{i=1}^{n} B_i\beta_i^3\right) - M_1^2 \qquad (10)$$

It can also be shown that the estimate of the steady-state quantity of xenon in the organ after a very long exposure to inspired xenon can be expressed as

$$Q_\infty = GF \sum_{i=1}^{n} B_i\beta_i^2 \qquad (11)$$

The analysis serves to separate the intensive, time-independent quantity, Q_∞, from the kinetic information that is presented in the moments of f(t).

In our analysis of the experimental data, we fitted each record of gas concentration vs. time to *Eq. 8* using a nonlinear least-squares fitting routine based on the method of Marquardt (14). In most cases the fit was satisfactory when two exponential terms were used (cf. Fig. 1), but usually three and, occasionally, four terms provided a better fit. In the three experiments with minimal experimental problems, a two-exponential form of *Eq. 7* was used to fit all data from locations that recorded at least 2,500 gamma events during the study.

Our earlier work (20) included a specific term, the lung-arterial time constant, to allow for transients before the tissue level. That more complete analysis was applied to several dozen data sets from the present report. In roughly half these data sets, the improvement in fitting data was insufficient to pass an F test for significance of improvement. In the other sets, the time constant found was in the range of 0.5–1.0 min. Now, in a serial process like the serial delivery of gas to the lungs, the arteries, and the tissues; the mean and variance of the overall process is simply the sum of the individual means and variances. Neglect of the delivery transit in describing tissue transfer will produce an overestimate of tissue mean and variance by the lung-arterial values. In the present work the adjustment is seen to be small and close to the precision of the tissue estimates themselves. Thus the delivery transit was ignored, and the simpler *Eq. 8* was used for all data presented. This provides a uniform method of analysis for all data whether or not it is possible to estimate small contributions from the delivery process.

RESULTS

Examples of raw data curves are presented in Fig. 1. The curves are from the same experiment as presented in Figs. 2, 5, 8–11, and 13. The area labeled brain is the composite of 40 contiguous spatial regions over the center of the skull and the area labeled shoulder contains 49 contiguous spatial points over the scapula-humerus joint. The smooth curves are the result of fitting a two-exponential form of *Eq. 8* to the data.

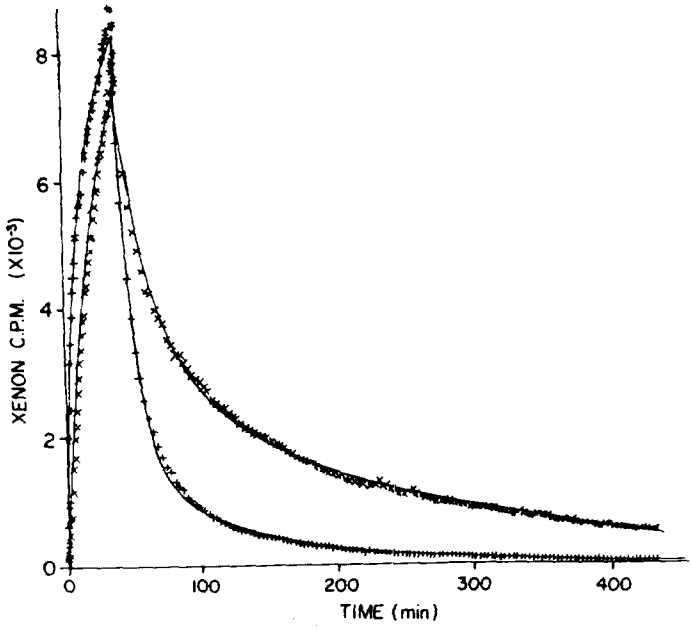

FIG. 1. Examples of raw data curves from *expt 10*. Dog breathed 11 mCi/l ^{133}Xe for 40 min and room air for the following 6 h. Time course of xenon concentration is shown in dog's brain (+) and shoulder (×). Smooth curves are best-fit lines to *Eq. 8* using a 2-exponential form of f(t) in *Eq. 7*.

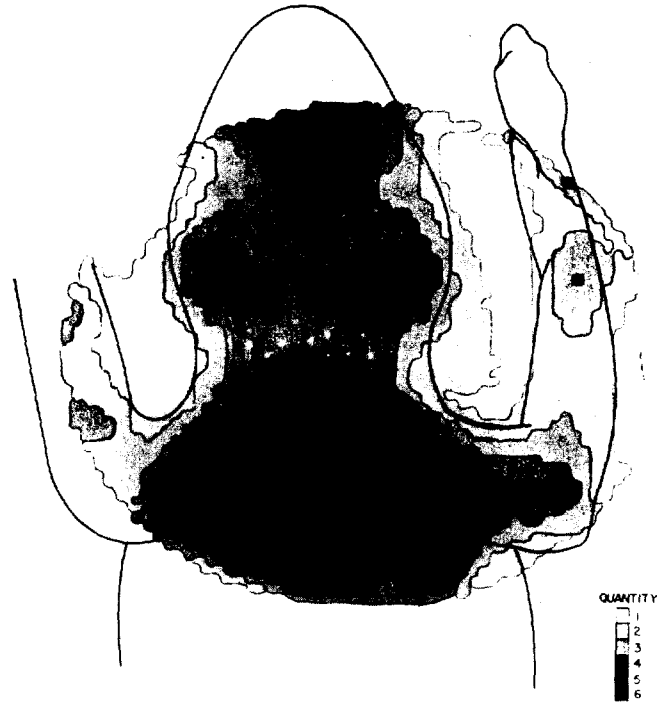

FIG. 2. Map of steady-state xenon quantity in dog upper extremities from *expt 10*. A 6-point gray scale is used based on 6 equal intervals of quantity (in cpm) with the highest value found in the study defining upper limit of darkest area (*shade 6*) and zero as lower limit of lightest area (*shade 1*). Dog's eyes are just inside upper edge of field; right forelimb is within field to level of ankle joints; left forelimb is only partially in field. Dark area in head is in line with positions recorded at right external ear.

Gas capacity. The local variation in gas exchange characteristic of the dog can be seen in the set of functional "maps" obtained from the three experiments that allowed a full analysis. The measure of gas capacity that is independent of kinetics is the estimated steady-state xenon quantity in each location defined in *Eq. 11.* Maps of gas capacity are shown in Figs. 2–4. This parameter is the predicted equilibrium xenon capacity, which is the product of gas solubility in the tissue and the volume of tissue "seen" by the measuring device. In these experiments the volume is determined by gamma-camera resolution and collimation, by the thickness of tissue, and by the distance from the camera face. With the complicated dependence on geometry, only those areas of the dog thicker than about 5 cm and equidistant from the camera will have a roughly equivalent volume. Under these conditions, gradients in steady-state quantity can be directly interpreted as differences in average xenon solubility.

Figure 2 shows the steady-state quantity over the upper extremities of a single dog that inspired 11 mCi ^{133}Xe per liter of O_2 for 40 min. A total of 2,311 areas met the statistical requirement for curve fitting (a total of 2,500 gamma counts per area had to be recorded during the entire study). Precision of the estimated steady-state quantity (precision is defined as the ratio of the standard error of a parameter to the estimated value of parameter) was very good: 2,291 areas had better than 5% precision.

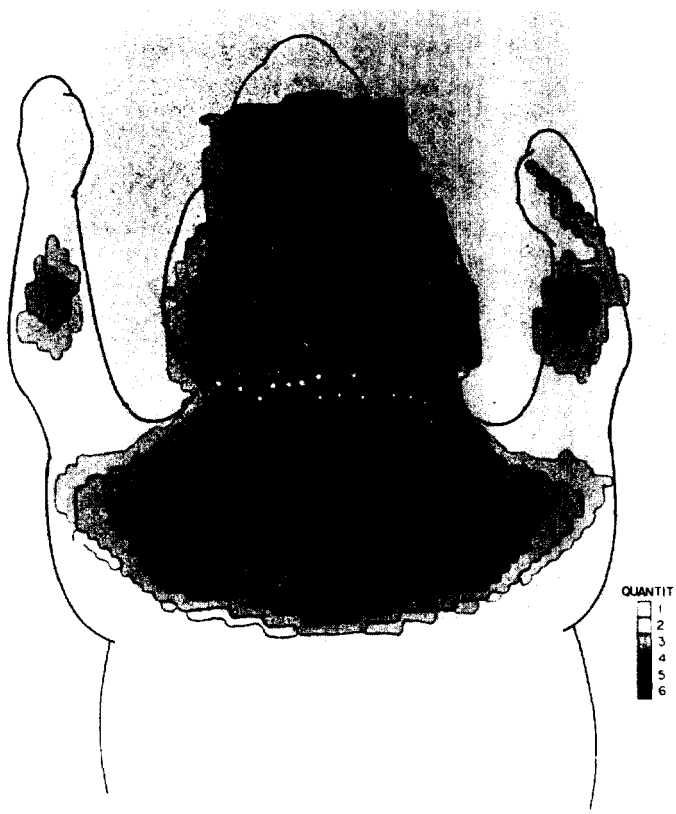

FIG. 3. Map of steady-state xenon quantity in dog upper extremities from *expt 9.* Gray scale is established in same way as in Fig. 2. Dog's eyes were at upper edge of field; shoulders were in center of darkest areas in bottom third; both forelimbs up to wrist joints were also included.

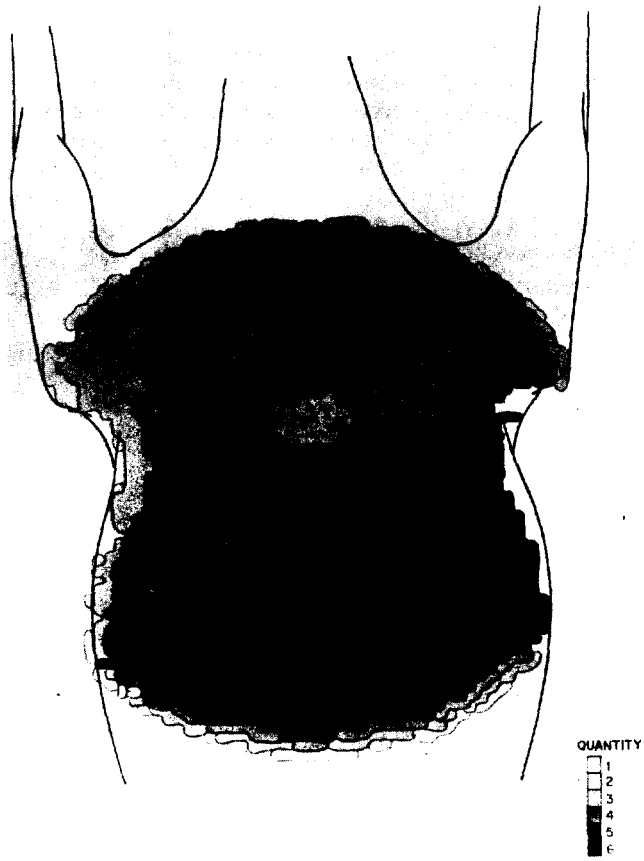

FIG. 4. Map of steady-state xenon quantity in dog trunk from *expt 6.* Gray scale was established in the same manner as in Figs. 2 and 3. Shoulders were just inside field of view at top, and kidneys were just inside bottom of field.

For clarity, the full resolution is not presented in the figures. Rather, for the maps of steady-state xenon quantity, a six-level gray scale that corresponds to equal increments of the full range of values found in all 2,311 areas is used. Darkest areas in Figs. 2–4 represent the highest xenon gas capacity found in the studies. The areas of highest steady-state quantity are in and near both shoulder joints. The remainder of the upper trunk has a relatively high gas capacity. The brain, an area thick enough for comparison with the trunk, has a lower steady-state capacity than the shoulders by a factor of one-half to one-third, which probably means a lower coefficient of solubility. The forelimb overall appears to have a relatively low capacity, but, because it is relatively "thin," direct comparison with head and trunk is impossible. Note that the joints in the limb have a high gas capacity compared to the nearby areas of muscle and long bone.

Figure 3 is a map of the steady-state concentration of another dog. This animal inspired 6.5 mCi ^{133}Xe per liter of O_2 for 40 min. A region similar to that shown in Fig. 2 was chosen but the lower amount of isotope used in this study produced only 1,903 areas suitable for analysis. Precision was also good: 1,630 areas were better than 5% and only 16 areas were worse than 10%. As in Fig. 2, the highest xenon capacity is also found near the shoulders

with other high values found in other joints. Note also the slightly higher values near the inner ears compared to the rest of the relatively low steady-state quantities in the brain. The cervical spine also appears to have a rather high xenon capacity compared to the rest of the upper trunk.

Figure 4 is a map of a different region studied in another dog. This animal inspired 4.4 mCi ^{133}Xe per liter of O_2 for 50 min; 2,079 areas were suitable for curve fitting. The precision of estimated steady-state quantity was not as good as that shown in Figs. 2 and 3: 1,869 areas were better than 5%, but 108 were worse than 10%. Most of the imprecise estimates were obtained near the upper edge of the image and were caused by a slight rotation of the dog's head midway through the study. Even though the thorax is "thick" to xenon, relative values of steady-state quantity cannot be taken as solubility differences because the gas spaces of the lung contribute significantly to the quantity of xenon measured and only insignificantly to the absorption of gamma rays. Once again, a relatively high capacity for xenon is seen in the shoulders as well as in the kidneys.

Mean residence time. Maps of estimated mean residence time of xenon, defined by *Eq. 9*, are shown in Figs. 5–7. The gray scale is based in intervals of minutes (see keys in figures). The precision of the calculated mean times in Fig. 5 (the same experiment as shown in Fig. 2) are good: 1,868 areas are better than 5%, and only 46 are worse than 10%. The center of the brain is clearly the fastest area for gas exchange with mean times under 10 min. The eyes are slower in gas exchange by about a factor of three. The inner ears are roughly 5 times slower than other brain areas. Most of the upper trunk has a moderate mean residence time of 20–50 min, but the shoulders have a very long gas exchange rate: over 1.5 h.

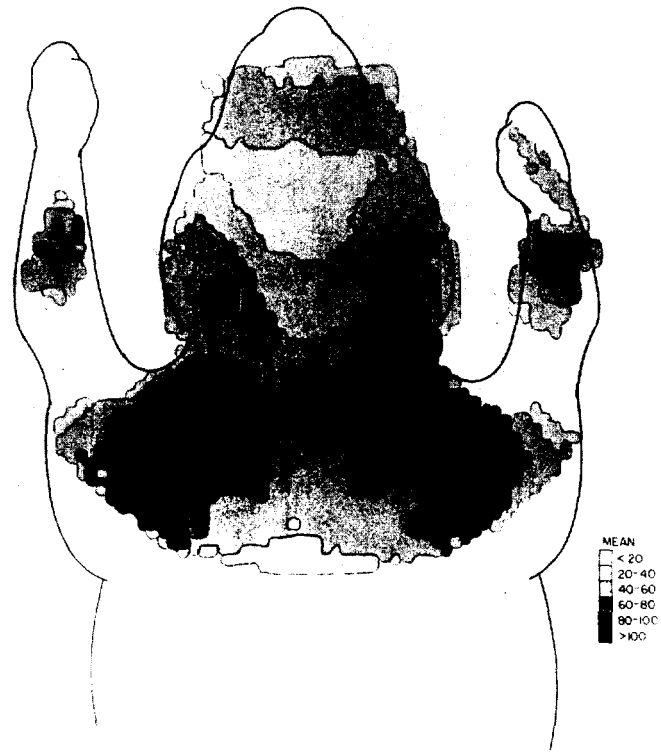

FIG. 6. Map of mean residence time in dog upper extremities from *expt 9*. Gray scale indicates range of times in min.

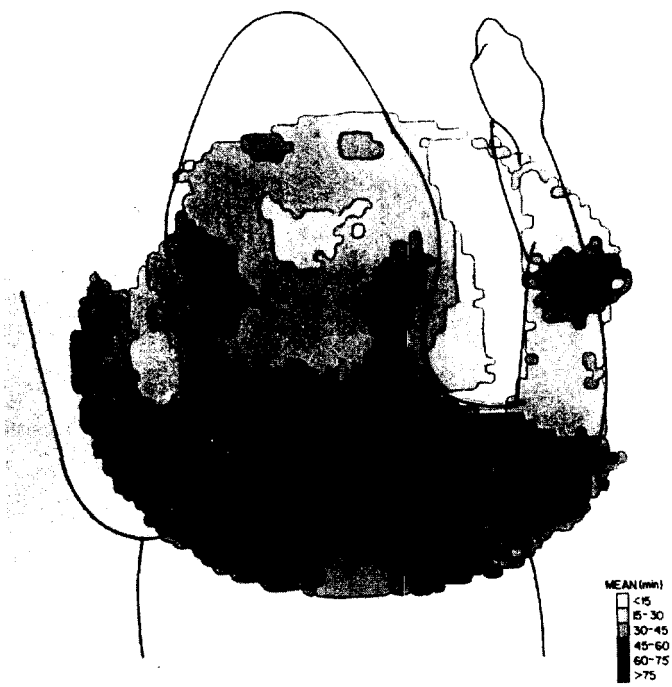

FIG. 5. Map of xenon mean residence times in dog upper extremities from *expt 10*. Gray scale indicates range of times in min.

The mean residence times of another dog are mapped in Fig. 6. The precision is good: 1,630 areas were better than 5%, and only 16 were worse than 10%. The ranking of gas exchange rates by organ appears to be the same as in Fig. 5. The center of the brain is fastest, followed by nonjoint areas of the forelimb, limb joints, and ear, and finally, by the very slowly exchanging shoulder joints.

Mean residence times in the dog's trunk are shown in Fig. 7. The precision of this parameter in this dog is generally poorer than the other two: only 239 areas are better than 5%, 1,761 are better than 10%, and 150 are worse than 25%. Once again, the shoulder joints are the slowest exchanging tissues with mean residence times over 2 h. Gas exchange is markedly faster in areas approaching the lungs. The lungs themselves have mean times under 5 min, as expected. Neither the heart nor the kidneys have distinctive exchange rates, but the region below the lungs near the liver appears rather slow.

The point-to-point variations in mean residence times shown in Figs. 5–7 appear to be the most sensitive way to establish anatomic differences in gas exchange. To present the mean residence times mapped in Fig. 5 in more detail, we have plotted two sections of that map in Figs. 8 and 9. In Fig. 8 the mean residence time is plotted

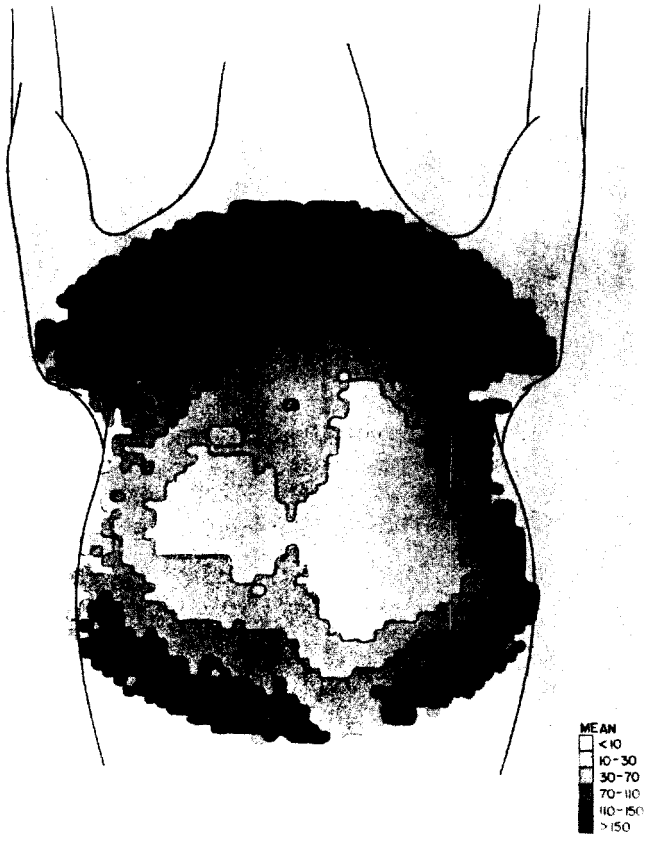

FIG. 7. Map of mean residence time in dog trunk from *expt 6*. Gray scale indicates range of times in min.

along a line parallel with the spine, but offset to include the right shoulder, right ear, and right eye. The error bars are 95% confidence limits on the estimated mean times. Except where the areas include sharp gradients, as the edges of the shoulder, the mean times are quite precise. The very slowly exchanging shoulder is clearly seen, as are the peaks representing the relatively slow ear and eye.

Figure 9 is a similar plot of mean residence time along a transverse section perpendicular to the one chosen for Fig. 8. This plot shows the long residence times found in both shoulders. Note also the slower exchange rate over the left humerus bone compared with the more rapid gas exchange in the muscle and connective tissue that are located between the shoulder and forelimb in this position. The intersection of the two lines used for Figs. 8 and 9 occurs just posterior to the center of the dark shading of the right shoulder in Fig. 5, so that the values of the maximum residence time in the shoulder of Figs. 8 and 9 do not exactly coincide. The large error bars on Fig. 9 at the edges of the shoulder indicate that summing data over larger areas will lead to loss of precision in estimates of exchange kinetics.

In addition to the point-by-point variability in mean residence time, there is a significant variation in repeated measurements in a single animal and among different animals. We obtained information on biological and experimental variability of exchange by pooling data of the three studies just presented in detail with the other six

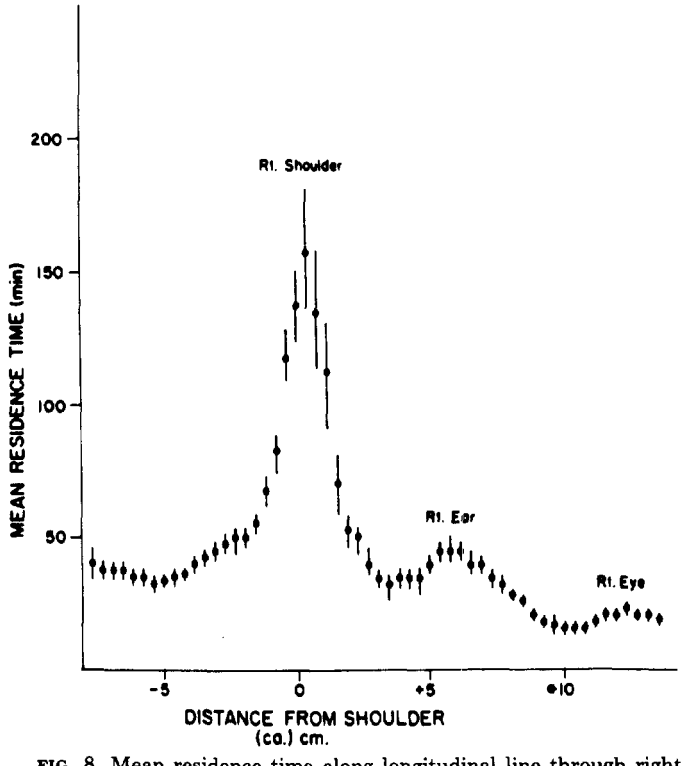

FIG. 8. Mean residence time along longitudinal line through right shoulder of dog in *expt 10*. *Circles* are estimated times; *error lines* extend 2 SE above and below estimate. *Abscissa units* refer to approximate distance in cm.

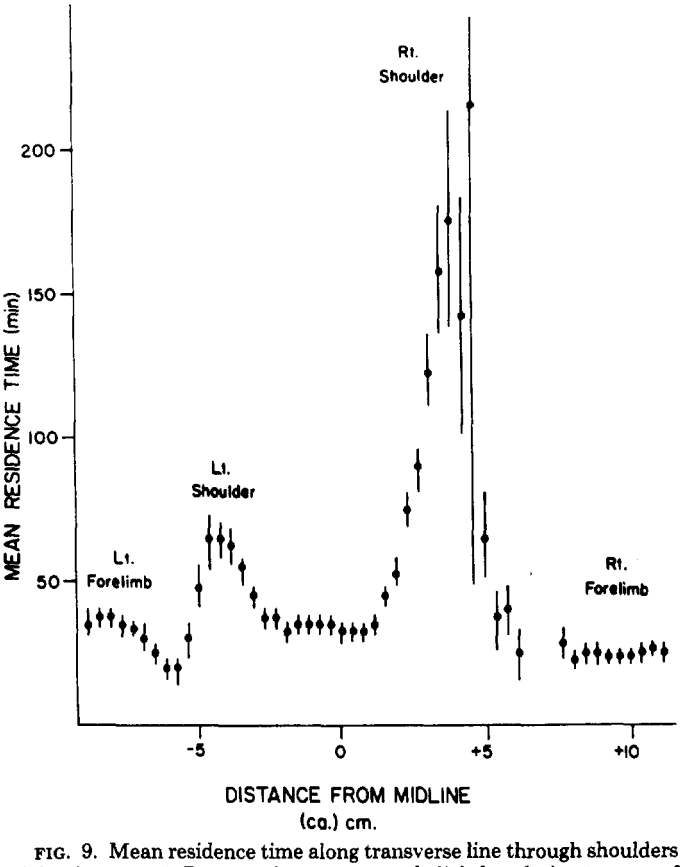

FIG. 9. Mean residence time along transverse line through shoulders of dog in *expt 10*. Because dog was rotated slightly relative to axes of gamma camera, line does not extend through center of left shoulder area. *Circles* are estimated times; *error lines* extend 2 SE above and below estimate. *Abscissa units* refer to approximate distance in cm.

that had degraded spatial resolution. For each of the nine studies, raw data from medium size areas (30–60 of the smallest areas; 7–15 cm^2) were combined into data sets that referred to a given anatomic area, e.g., an eye. These combined data sets were analyzed as before and the results from all studies are summarized in Table 1.

The experiment-to-experiment variability is severe, but some of the discrepancies appear to result from unequal precision in the estimate of mean residence time among experiments. The data sets for each anatomic region were averaged with a weighting inversely proportional to precision and the average mean times are plotted in Fig. 10. This weighting procedure accounts for up to half the apparent variability seen in Table 1. Nevertheless, the sharp tissue and organ differences in Figs. 2–7 have been overwhelmed by the day-to-day and animal-to-animal variability. Some of the variability is due to an inability to perfectly reconstruct the medium size areas of interest in different animals; the large spatial gradients apparent in Figs. 8 and 9 were not appreciated before this analysis. Anatomic sites should have been more precisely defined at the time of the experiment. Some of the regions are definitely different because of different animal positioning. For example, the repeated studies of *dog C* had different animal orientations: *expt 4*, lateral upper extremities; *expt 5*, ventral lower extremities; *expt 6*, dorsal trunk; *expt 7*, dorsal upper extremities. Finally, some of the variability must also be due to actual biological differences in the animal preparations, such as variable animal response to prolonged periods of rather heavy anesthesia (6).

Higher moments of the residence time distribution. Our analysis of tracer data using moments summarized the "equilibrium" or nonkinetic information in the steady-state gas quantity and the average overall exchange rate in the first moment. Details of tracer kinetics appear in the second and higher moments of the residence time distribution. Plots of the variance defined in Eq. 10 vs. the mean residence time in all areas of the two head and forelimb studies already presented are shown in Figs. 11 and 12. The corresponding plot for the upper trunk study is not presented because the large number of areas that include gas phase in the lung have large variances (second moment) that arise from the mixture of lung and tissue samples. Two points are evident: first, there is a very strong correlation between first and second moments. This correlation may lead in time to a fairly simple mathematical description of the exchange curve that has useful predictive properties (9). The second is that the lines of correlation, and, indeed, nearly all the individual points, have much higher variances than would have resulted from a single flow-limited compartment ("perfusion-limited" exchange) in each of the roughly 2,000 areas presented in each graph.

The actual value of the second moment is important because it is a measure of how much gas leaves an anatomic region at a time far from the average time. For map presentation, the variances are normalized by the square of the mean residence times. This normalization is appropriate because the normalized value is independent of the units of time employed, and because the correlations shown in Figs. 11 and 12 indicate that variance depends on mean by a power not much less than 2. Figures 13 and 14 are maps of normalized variance for the dog studies already shown. The value of normalized variance in most areas is in the range of 3–5; in fact, 66% of the areas in both of these studies fall between these values. The dog whose trunk was studied had only 28%

TABLE 1. *Mean residence time variability among experiments*

Expt	Animal	Eye	Brain	Spine	Shoulder	Knee	Long Bone	Wrist
2	*A*					450.	108.1	58.4
						±520.	±4.9	±3.7
							374.	
							±7.	
3	*B*	21.7	33.1		99.8	184.	66.6	
		±0.4	±0.5		±65.	±140.	±3.3	
		40.1	36.1					
		±0.7	±1.2					
4	*C*	32.9	29.1	402.		318.	235.	459.
		±1.1	±0.9	±317.		±17.	±20.	±186.
			53.9	351.			117.	
			±2.9	±20.			±4.	
5	*C*						130.	
							±5.	
6	*C*			41.1	115.			
				±3.5	±14.			
7	*C*	21.7	14.0	99.8	202.	47.1	43.2	
		±0.6	±0.5	±3.4	±48.	±2.2	±1.4	
		24.6			125.	119.	74.5	
		±2.7			±11.	±39.	±6.1	
8	*D*	29.3	16.6	27.5			45.6	27.4
		±0.3	±0.4	±0.6			±0.7	±0.4
		24.3					56.1	34.8
		±0.4					±0.7	±0.5
9	*E*	20.1	16.5	48.4	120.		43.2	26.0
		±0.3	±0.2	±10.5	±2.		±1.9	±1.8
		18.5			130.		32.1	19.2
		±0.4			±910.		±1.3	±1.1
10	*F*	25.2	13.5	31.2	74.9	46.5	27.7	20.3
		±0.4	±0.3	±0.8	±2.4	±1.0	±0.5	±0.5
		23.0			75.6			
		±0.4			±1.9			

Values are means ± SE of the estimate in minutes. SE used in plotting Fig. 10 were obtained by considering each column of Table 1 as a set of independent estimates of a population; overall population mean and variance were then calculated by weighing each entry inversely as the individual precisions of the means. Spine includes regions of thoracic and cervical spine but no lumbar regions. Long bone includes regions of tibia and femur, several cm away from the joints.

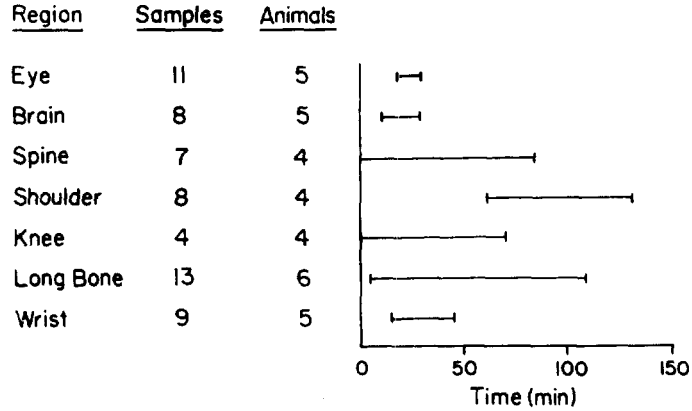

FIG. 10. Estimates of mean residence times in various organs for entire dog population. Means and SE of all experiments listed in Table 1 were combined for estimation of mean and SD for overall dog population; weights for each tabulated value were taken as inversely proportional to entry precision. *Bars* extend 1 SD above and below the population mean.

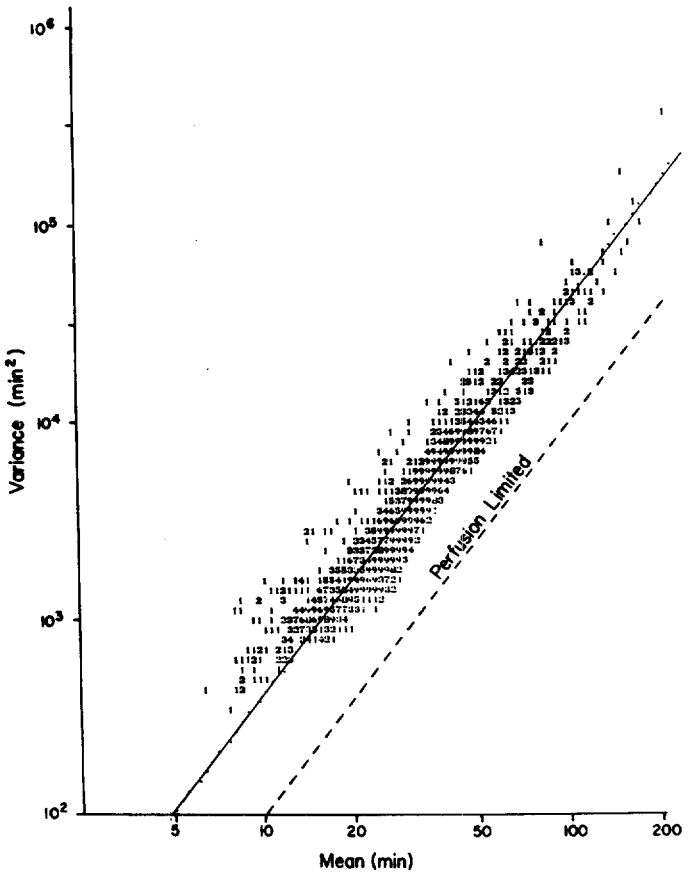

FIG. 11. Dependence of variance (2nd moment) on mean residence time (1st moment) for all dog areas from *expt 10. Numbers* refer to number of anatomic locations that have the indicated coordinates (total points = 2,311). *Solid line* obtained by log-log regression plotted through data is variance = 4.61 (mean)$^{1.97}$. *Dotted line* is expected result for individual flow-limited compartments where, theoretically, variance = 1.0 (mean)$^{2.00}$.

in the range, but that study included many areas composed of mostly pulmonary gas space and some overlying tissue that would produce broad exchange curves. Thus, most tissue curves have approximately the same "width." The more highly dispersed gas exchange rates, the higher relative variance values, are found near the center of the brain and along the cervical spine.

DISCUSSION

This study has addressed the biological exchange of an inert gas by considering several levels of variability: the variation in the time required for a tracer to emerge from a single anatomic site, the variation in exchange rates among anatomic sites, and the variation in rates found in different animals. Presenting the results of this study has naturally involved the application of certain statistical measures.

Description by moments of a single raw data curve of gas exchange has been discussed previously (20). In the present work two very important advantages of the method have emerged. The likelihood of encountering different mechanisms of gas exchange increases when thousands of gas exchange sites are examined. Because the moments do not follow any single model of exchange mechanism, the resulting characterization of rate differences is not clouded by the application of a model unsuitable for the tissue in question. The second clear advantage is the concise nature of moments as summary descriptions. The thousands of organ areas studied simultaneously need to be compared by a small number of meaningful parameters. Our use of steady-state quantity and the mean and variance of the residence time distribution function provides such a summary useful for area-by-area contrast. Use of exponential terms, however, is much more involved because the parameters covary so highly. For example, the "fast" time constant for any area depends heavily on the value of the "slow" time constant, as well as on the weighting for each term and even the number of terms chosen for the fit (the n in *Eq. 7*).

Application of the analysis is not without hazard. Both the model used for the residence time distribution (*Eq. 8*), and the data must have certain qualities for the means and variances of the organ to be reliably recovered. The actual shape of $f(t)$ in each tissue is an unknown function that can only be estimated by data. If, for example, the actual function had a "spike" immediately following the last observation, these procedures would fail to obtain the physiologically correct parameters. The problems of extrapolating to infinite times will be especially prone to

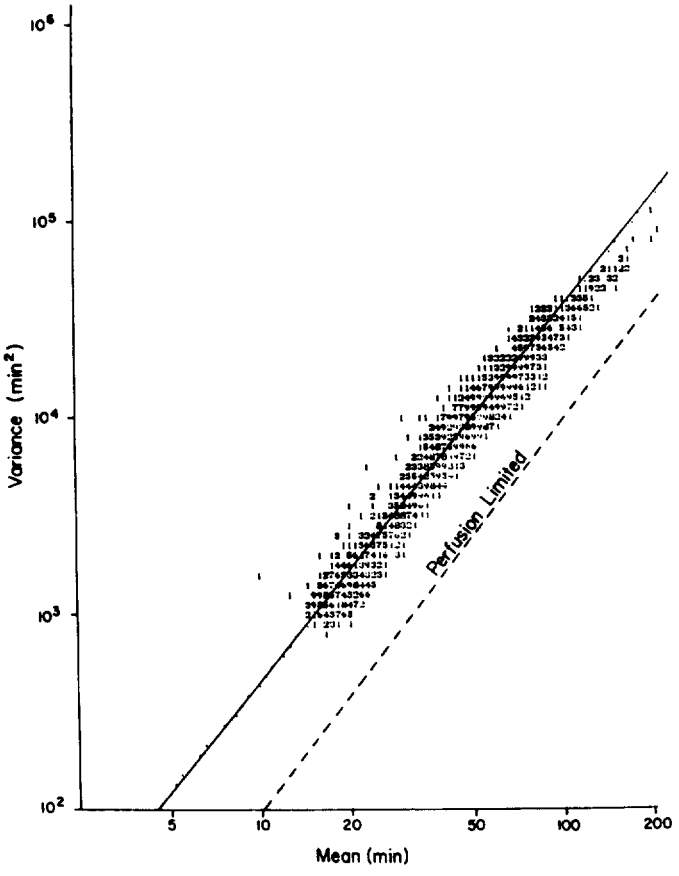

FIG. 12. Dependence of variance (2nd moment) on mean residence time (1st moment) for all dog areas from *expt 9. Numbers* refer to how many anatomic locations have the indicated coordinates (total points = 1,903). *Solid line* obtained by log-log regression and plotted through is variance = 6.89 (mean)$^{1.86}$. *Dotted line* is expected result for individual flow-limited compartments where, theoretically, variance = 1.0 (mean)$^{2.00}$.

bias and were discussed in the earlier report (20). Sufficiency of data must be such as to provide both satisfactory tests of the shape of the presumed function as well as to precisely estimate the moments in the presence of experimental error or "noise." The numerical procedures employed in the estimation procedure, a well-known nonlinear fitting algorithm in our case, will in general also introduce some degree of bias in the estimates. Some of these problems are demonstrated by numerical examples in the APPENDIX. Changes in the span of data taken, the models fitted to the data, or the methods of fitting may each alter estimates of the moments. The chief aim in this paper is to compare adjacent regions of tissue by means of moments estimated with the same model, data collected over the same period of time, and fitted by the same algorithm. It is therefore reasonable to expect that the biases will be of similar size and that the relative magnitude of the moments will not be altered much by these factors. Comparison with other studies conducted and analyzed in a different manner would, of course, be more complicated.

Figures 2–4 present the maps of a parameter (the steady-state gas quantity) that is a complicated sum of xenon tissue solubility and geometrical factors. The geometry is such that comparisons of solubility can only be made among nearly contiguous points. Actual numerical determination of gas solubility is not feasible with a gamma camera without extensive calibration experiments. Subject to these limitations, the data do indicate a higher xenon solubility in areas of joints, ears, and spine than in adjoining regions.

FIG. 14. Map of (variance/(mean)^2) in dog upper extremities for *expt 9*. Gray scale corresponds to integer ranges for this (dimensionless) normalized variance.

FIG. 13. Map of (variance/(mean)^2) in dog upper extremities for *expt 10*. Gray scale corresponds to integer ranges for this (dimensionless) normalized variance.

A number of studies have determined xenon solubility in tissues by more direct methods. The tissue-blood partition coefficient is in the range of 0.6–0.8 for skeletal (1, 4, 15, 18, 21) and cardiac (1, 4) muscle, kidney (1, 4), liver (1, 4, 13), eye (5), and brain (1, 18, 21). Slightly lower values have been reported for cerebrospinal fluid (19) and synovial fluid, tendon, and cartilage (15). The hard tissues with high solubility in the present study apparently have not been studied elsewhere.

In contrast to the steady-state quantity, the moments of the residence time function do not depend upon camera or animal alignment. These measures are time averages that are independent of the scale of measurement in the same way that the half time of a truly exponential curve is independent of scale. One measurement peculiarity remains, however. In all external measurement of in vivo distribution of isotopes, the signal arriving at the camera is composed of gamma rays emitted from many depths in the tissue up to a maximum of several centimeters. All data, for example, are composed partially of gas kinetics of overlying skin. Regional differences are nevertheless seen in the figures, which show data from the underlying organs.

Mean residence times in the dog were found to vary over two orders of magnitude: from about 2 min in the lungs to 2 h in the shoulder joints. This separation of

exchange rates appears feasible only when a large number of anatomic sites can be examined simultaneously: day-to-day and individual-to-individual differences can overwhelm moderate organ-to-organ variations. The order of mean exchange rates within an animal appear to remain consistent as

lung > brain > eye ~ spine ~ leg > ear

> peripheral joint > shoulder

(ranked from fastest to slowest exchange).

Comparison of these exchange rates with other studies is very difficult. Though numerous experiments on xenon-tracer kinetics have been published, most of these have been studies of "local blood flow." The overwhelming majority of experiments reported have assumed tissue diffusion equilibrium for the gas and have published only one or two half times or flow rates. Even though most models of tissue gas exchange predict that mean residence time should be simply the ratio of tracer volume of distribution to tissue blood flow (9, 17), few xenon "flow" studies present sufficient data to use this relationship. Of the fewer number of studies that show actual data, most are not useful because the data collection ignored the first few minutes of rapidly changing gas concentration or ignored all slowly changing concentrations after an arbitrarily short period such as 15 min. The remaining suitable data show xenon mean residence times of a similar magnitude or somewhat shorter than the present study: 1.2–26 min in muscle (16); 15 min in the forearm (8); 35 min in the knee joint (15); 3–12 min in the heart (3); and 4 min in the brain (7). In the latter five reports different analyses were used, but each report included a suitable plot of raw data that we could then digitize and subject to an analysis similar to the one in the present study.

The information in the variance (and higher moments) in the residence time functions is difficult to interpret intuitively. We can oversimplify a bit and consider the mean time as the "position" of a residence time curve and the variance as the "width" of the curve. The width, i.e., variance of a single well-mixed compartment, is exactly equal to the square of its mean residence time. Figures 11 and 12 and thousands of other curves analyzed in this study have not produced any variance that small. In fact, most of our data give a ratio of variance to mean squared of 4 ± 1. Such a narrow spread in this parameter implies a general similarity in xenon residence time functions among widely varying organs. A similarity in shapes of other tracer curves also has been noted by Bassingthwaighte and Ackerman (2). No present theory of tracer kinetics seems able to reconcile the variance of residence times from this study to basic capillary physiology, but theories to address this point are under development (9).

It is reasonable to expect variability in microvascular physiology to be reflected in the variance of the gas residence times. The present data can be used to explore the effective size scale of such anatomic and physiologic variability. If one wishes to view local gas exchange as a single well-mixed (perfusion-limited) compartment, then none of the thousands of sites studied here is homogeneously perfused (cf. Figs. 11 and 12). Thus externally detected radioisotope techniques with resolutions down to about 1 ml may never allow discovery of such compartments, if they actually exist. The relative importance of larger area inhomogeneity may also be examined. When the data of single animals are reanalyzed by combining areas into new areas larger by factors of 9, 25, or 64, effectively redoing the study at progressively lower spatial resolution and studying larger tissue volumes, the ratio of variance to mean square remains at 4 and the parameter becomes even more sharply estimated (87% of the 64-fold larger areas have a value of 4 ± 1). This unexpected result indicates that the size scale of heterogeneity important to gas transfer occurs on a scale smaller than sizes of 1 ml.

The present study appears intriguing in its implication for decompression sickness. The "special" anatomic areas for gas exchange, the middle ears, shoulders, and peripheral joints, are specifically those sites involved in the symptoms of decompression sickness (11). Judged from the present data, it appears feasible with existing techniques to construct concentration-time profiles that will predict which organs have comparatively high gas tensions at any given time in a particular pressure-decompression maneuver. The steady-state quantity, the mean, and the variance of any gas exchange equation used should be appropriately matched to the values characteristic of the tissue. Furthermore, the strong correlation between variance and mean may imply that reliable gas exchange predictions can be developed with only a single kinetic parameter.

APPENDIX

Some of the numerical problems associated with approximating an unknown physiological function with a simple analytical function can be examined using synthetic data sets. Four such data sets were constructed, all using nine exponential terms in series. The parameters used are presented in Table 2. The time constants are spread over the range likely to be detected by the experimental observations obtained (5–720 min) and are chosen to be those used in traditional calculations for decompression table design. The coefficients were adjusted (by trial and error) to meet the constraint of *Eq. 6* in the text and to approximate the parameter values found in the actual dog studies. For comparison, the average steady-state gas quantity, mean, and variance in experiment 10 were 219 cpm, 35.1 min, and 6,504 min, respectively; and in *expt 9* they were 239 cpm, 53.5 min, and 13,360 min. Synthetic data *set A* is a close approximation of the average of the parameters of these two experiments, *set B* has a variance 50% higher, *set C* a mean 50%

TABLE 2. *Parameters used in constructing synthetic data*

Term	Time Constant (β_i), min	Weight ($B_i\beta_i$)			
		Set A	*Set B*	*Set C*	*Set D*
1	5	0.020	0.040	0.020	0.032
2	10	0.164	0.180	0.100	0.175
3	20	0.400	0.438	0.160	0.210
4	40	0.280	0.250	0.250	0.190
5	75	0.080	0.040	0.334	0.200
6	120	0.030	0.020	0.115	0.160
7	240	0.016	0.014	0.015	0.019
8	480	0.006	0.010	0.004	0.010
9	720	0.004	0.008	0.002	0.004
Mean		40.14	40.08	60.11	60.15
Variance		10,152.	15,124.	10,050.	14,997.

TABLE 3. *Results for synthetic data set A estimates and standard errors*

Run	Steady State	Mean	Variance	SE Fit
1	218.9 ± 3.1	41.3 ± 1.2	5,440 ± 370	1.21
2	221.6 ± 3.6	43.7 ± 1.4	6,290 ± 580	1.29
3	221.8 ± 3.1	41.4 ± 1.3	5,180 ± 330	1.23
4	223.7 ± 2.9	40.9 ± 1.1	5,280 ± 340	1.13
5	221.4 ± 3.2	45.5 ± 1.4	6,060 ± 430	1.21
6	221.0 ± 3.5	42.3 ± 1.4	5,950 ± 450	1.34
7	219.4 ± 3.3	39.9 ± 1.3	5,000 ± 320	1.31
8	220.9 ± 3.4	41.5 ± 1.4	5,520 ± 390	1.31
9	223.8 ± 3.5	43.0 ± 1.4	5,660 ± 450	1.30
10	221.6 ± 3.5	42.0 ± 1.3	5,870 ± 550	1.27
Average	221.4	41.7	5,630	1.26
Original	230.0	40.1	10,200.	1.25

TABLE 4. *Results for synthetic data set B estimates and standard errors*

Run	Steady State	Mean	Variance	SE Fit
1	211.9 ± 3.6	40.3 ± 1.3	7,250 ± 700	1.21
2	216.3 ± 4.6	43.1 ± 1.6	8,820 ± 1160	1.30
3	213.3 ± 3.5	40.3 ± 1.4	6,630 ± 570	1.24
4	216.1 ± 3.4	40.0 ± 1.2	6,950 ± 630	1.13
5	214.0 ± 3.7	44.5 ± 1.5	8,010 ± 790	1.21
6	214.5 ± 4.1	41.4 ± 1.6	7,930 ± 830	1.34
7	211.0 ± 3.6	38.8 ± 1.4	6,390 ± 560	1.31
8	213.5 ± 3.8	40.5 ± 1.5	7,200 ± 710	1.32
9	216.5 ± 4.0	42.0 ± 1.5	7,550 ± 840	1.30
10	216.3 ± 4.6	41.5 ± 1.5	8,320 ± 1140	1.27
Average	214.3	41.2	7,510	1.26
Original	230.0	40.1	15,100.	1.25

TABLE 5. *Results for synthetic data set C estimates and standard errors*

Run	Steady State	Mean	Variance	SE Fit
1	225.8 ± 2.9	62.1 ± 2.1	7,230 ± 350	1.18
2	228.1 ± 3.3	65.4 ± 2.2	8,020 ± 550	1.26
3	230.0 ± 3.0	61.7 ± 2.3	6,990 ± 320	1.22
4	230.9 ± 2.8	60.4 ± 2.0	7,010 ± 320	1.12
5	229.9 ± 3.1	69.3 ± 2.3	7,990 ± 450	1.20
6	228.1 ± 3.3	63.7 ± 2.5	7,810 ± 410	1.31
7	226.7 ± 3.1	58.6 ± 2.4	6,730 ± 310	1.28
8	228.3 ± 3.2	61.6 ± 2.4	7,330 ± 360	1.28
9	231.0 ± 3.3	64.3 ± 2.2	7,420 ± 430	1.28
10	227.4 ± 3.3	62.4 ± 2.0	7,520 ± 530	1.24
Average	228.6	63.0	7,410	1.24
Original	230.0	60.1	10,200.	1.25

TABLE 6. *Results for synthetic data set D estimates and standard errors*

Run	Steady State	Mean	Variance	SE Fit
1	220.2 ± 3.0	61.0 ± 2.4	9,020 ± 480	1.19
2	223.2 ± 3.5	66.2 ± 2.6	10,300 ± 730	1.28
3	224.1 ± 3.1	61.7 ± 2.6	8,800 ± 470	1.23
4	225.5 ± 2.9	61.0 ± 2.2	8,950 ± 480	1.13
5	224.5 ± 3.1	70.2 ± 2.7	10,200 ± 600	1.21
6	223.1 ± 3.4	62.5 ± 2.9	9,720 ± 580	1.32
7	220.7 ± 3.2	57.1 ± 2.8	8,280 ± 450	1.29
8	223.0 ± 3.3	60.9 ± 2.8	9,160 ± 530	1.30
9	225.4 ± 3.4	64.8 ± 2.6	9,450 ± 600	1.29
10	222.2 ± 3.4	63.1 ± 2.3	9,690 ± 710	1.25
Average	223.2	62.9	9,360	1.25
Original	230.0	60.3	15,000.	1.25

higher, and *set D* both parameter values 50% higher. The synthetic error was obtained by a random number generator set to give a Gaussian distribution of zero mean and a standard deviation of 125% of the expected counting error (in both experiments, the overall average error of all points was 125% defined in the same manner). Input function, convolution, and data spacing were treated as in text *Eq. 8* to obtain a similar data structure. Fitting programs were the same as used for the data of the manuscript.

Results from fitting synthetic data *sets A*, *B*, *C*, and *D* are summarized in Tables 3–6. Ten replicates of each set were used with different runs of random noise added to the smooth curves. The standard errors of the parameters are very similar to those found in the actual data. The standard error of the fit (SE Fit in the tables, the measure of departure from simple counting statistical variation) is virtually the same as the added noise. This implies that the fits are about as good as possible, i.e., extra exponential terms could not be extracted from data with this much random error. The recovered values of the steady-state quantity, mean, and variance of the original distributions are quite reasonable. Steady-state quantities are 1–7% lower than the "perfect" values; estimates of the mean are 2–5% high; and the variance is estimated low by 25–50%. We would expect estimates of variance, and especially the higher moments, to be progressively less reliable because these moments depend strongly on behavior of the residence time function at long times. Our experiments were not prolonged sufficiently to obtain good descriptions of the "tails" of the distribution, and the simple function used for fitting was not particularly well suited to stress long-term behavior. Overall, this numerical exercise shows a very reasonable recovery of experimental precision (regarding the random error) and a moderately high level of accuracy (regarding bias in estimates of the parameters), which is degraded with higher moments of the distribution.

The authors express their deep appreciation to A. H. Baldwin for running many of the computer calculations, to R. Hamilton for providing the ^{99m}Tc tracers, to E. Barron and his associates for handling the animals, and to M. M. Matzen for editorial assistance.

This work was part of Naval Medical Research and Development Command, Work Unit M0099.PN001.1180 and was partially supported under Research Work Unit MJ60421 of the Armed Forces Radiobiology Research Institute, Defense Nuclear Agency. The opinions and assertions contained herein are the private ones of the writers and are not to be construed as official or reflecting the views of the Navy Department or the Naval Service at large. The experiments reported herein were conducted according to the principles set forth in the "Guide for the Care and Use of Laboratory Animals," Institute of Laboratory Animal Resources, National Research Council, DHEW, Publ. (NIH) 78-23.

Received 25 March 1980; accepted in final form 23 January 1981.

REFERENCES

1. ANDERSEN, A. M., AND J. LADEFOGED. Partition coefficient of 133-xenon between various tissues and blood in vivo. *Scand. J. Clin. Lab. Invest.* 19: 72–78, 1967.
2. BASSINGTHWAIGHTE, J. B., AND F. H. ACKERMAN. Mathematical linearity of circulatory transport. *J. Appl. Physiol.* 22: 879–888, 1967.
3. BASSINGTHWAIGHTE, J. B., T. STRANDELL, AND D. E. DONALD. Estimation of coronary blood flow by washout of diffusible indicators. *Circ. Res.* 23: 259–278, 1968.
4. CONN, H. L., JR. Equilibrium distribution radioxenon in tissue: xenon-hemoglobin association curve. *J. Appl. Physiol.* 16: 1065–1070, 1961.
5. FISH, M. B., D. M. O'DAY, S. B. ARONSON, M. POLLYCOVE, AND A. COON. Disappearance of intravitreous 133-xenon. Its relation to

ocular blood flow. *Arch. Opthalmol.* 86: 314–320, 1971.
6. GROOM, A. C., S. H. SONG, Y. OHTA, AND L. E. FARHI. Effect of anesthesia on rate of N_2 washout from body stores. *J. Appl. Physiol.* 37: 219–223, 1974.
7. HOEDT-RASMUSSEN, E. Regional cerebral blood flow: the intra-arterial injection method. *Acta Neurol. Scand. Suppl.* 27: 13–79, 1967.
8. HOLZMAN, G. B., H. N. WAGNER, M. IIO, D. RABINOWITZ, AND K. L. ZIERLER. Measurement of muscle blood flow in the human forearm with radioactive krypton and xenon. *Circulation* 30: 27–34, 1964.
9. HOMER, L. D., AND P. K. WEATHERSBY. The variance of the distribution of traversal times in a capillary bed. *J. Theor. Biol.* 87: 349–377, 1980.
10. ISBISTER, W. H., P. F. SCHOFIELD, AND H. B. TORRANCE. Measurement of the solubility of xenon-133 in blood and human brain. *Phys. Med. Biol.* 10: 243–250, 1965.
11. KIDD, D. J., AND D. H. ELLIOTT. Decompression disorders in diving. In: *The Physiology and Medicine of Diving and Compressed Air Work* (2nd ed), edited by P. B. Bennett and D. H. Elliott. London: Bailliere & Tindall, 1975, p. 471–495.
12. KITANI, K. Solubility coefficients of 85-krypton and 133-xenon in water, saline, lipids and blood. *Scand. J. Clin. Lab. Invest.* 29: 167–172, 1972.
13. KITANI, K., AND K. WINKLER. In vitro determination of solubility of 133-xenon and 85-krypton in human liver tissue with varying triglyceride content. *Scand. J. Clin. Lab. Invest.* 29: 173–176, 1972.
14. MARQUARDT, D. W. An algorithm for least-square estimation of nonlinear parameters. *J. Soc. Ind. Appl. Math.* 11: 431–441, 1963.
15. PHELPS, P., A. D. STEELE, AND D. J. MCCARTY. Significance of xenon-133 clearance rate from canine and human joints. *Arthritis Rheum.* 15: 360–370, 1972.
16. SEJRSEN, P., AND K. H. TONNESEN. Inert gas diffusion method for measurement of blood flow using saturation techniques. *Circ. Res.* 22: 679–693, 1968.
17. SPALDING, D. B. A note on mean residence-times in steady flows of arbitrary complexity. *Chem. Eng. Sci.* 9: 74–77, 1958.
18. TONNESON, K. H., AND P. SEJRSEN. Inert gas diffusion method for measurement of blood flow. Comparison of bolus injection to directly measured blood flow in the isolated gastrocnemius muscle. *Circ. Res.* 20: 552–564, 1967.
19. VEALL, N., AND B. L. MALLETT. The partition of trace amounts of xenon between human blood and brain tissues at 37°C. *Phys. Med. Biol.* 10: 375–380, 1965.
20. WEATHERSBY, P. K., E. E. P. BARNARD, L. D. HOMER, AND K. G. MENDENHALL. Stochastic description on inert gas exchange. *J. Appl. Physiol.: Respirat. Environ. Exercise Physiol.* 47: 1263–1269, 1979.
21. YEH, S. Y., AND R. E. PETERSON. Solubility of krypton and xenon in blood, protein solutions, and tissue homogenates. *J. Appl. Physiol.* 20: 1041–1047, 1965.